photonics

MDPI

Article

Aperiodic Frequency-Agile Optoelectronic Hybrid Oscillator

Tong Yang [1], Tengfei Hao [2,3,4], Yiwen Lu [5], Feifei Yin [1], Kun Xu [1], Ming Li [2,3,4] and Yitang Dai [1,*]

[1] State Key Laboratory of Information Photonics and Optical Communications, Beijing University of Posts and Telecommunications, Beijing 100876, China
[2] State Key Laboratory of Optoelectronic Materials and Devices, Institute of Semiconductors, Chinese Academy of Sciences, Beijing 100083, China
[3] College of Materials Science and Opto-Electronic Technology, University of Chinese Academy of Sciences, Beijing 100049, China
[4] School of Electronic, Electrical and Communication Engineering, University of Chinese Academy of Sciences, Beijing 100049, China
[5] School of Communication Engineering, Hangzhou Dianzi University, Hangzhou 310018, China
* Correspondence: ytdai@bupt.edu.cn

Abstract

In modern radar and electronic countermeasure systems, frequency-agile (FA) signal generators with low phase noise are of vital importance. The optoelectronic oscillator (OEO) is restricted by the periodic boundary condition (PBC), despite its superior performance in phase noise and frequency tunability. This paper proposes a new FA optoelectronic hybrid oscillator scheme, which employs a reconfigurable aperiodic FA filter and a dynamic frequency compensation module to collaboratively break the PBC limitation. It achieves fast switching and fine-grained frequency hopping at the 100 kHz level while maintaining low phase noise. Theoretical and experimental verification show that the system can generate arbitrary FA radio frequency (RF) signals from 1.95 GHz to 2.05 GHz with a tuning range of 10^3 times the free spectral range (FSR), and the phase noise reaches −120 dBc/Hz at 10 kHz offset. This study provides a novel technical route for generating narrow-step frequency-agile signals and effectively improves target detection accuracy and anti-jamming performance in electronic warfare applications.

Keywords: aperiodic frequency agility; low phase noise; frequency-agile signal generation; periodic boundary condition

1. Introduction

Modern radar and communication technologies hold an irreplaceable position in significant military and civil applications. Among various radar systems, frequency-modulated continuous wave radar is particularly outstanding because it can precisely acquire both target speed and distance at the same time, making it one of the most important detection devices in practical engineering [1,2]. As modern electromagnetic environments become increasingly complex and contested, radar and communication systems are facing severe threats from electronic countermeasures, including intentional jamming, deceptive repeaters, and spectrum interception [3]. As application scenarios continue to expand and diversify, radars are increasingly required to possess strong jamming resistance and anti-interference capabilities to ensure the safety and reliability of information transmission [4–6]. Fast frequency-hopping signals can effectively widen the detection dynamic range and strengthen clutter suppression; meanwhile, low phase noise helps reduce the error between measured data and real targets, thus significantly improving the precision and stability

Received: 27 May 2026
Revised: 15 June 2026
Accepted: 17 June 2026
Published: 19 June 2026

of the whole detection system. For this reason, the frequency agility and phase noise performance of microwave signals have become two core evaluation indices for advanced radar systems [7,8].

Traditional electronic methods commonly adopt schemes such as direct digital synthesis (DDS), phase-locked loop (PLL) combined with voltage-controlled oscillator (VCO), or digital frequency synthesizers [9], but the accuracy of such methods is susceptible to temperature and noise interference [10]. To address the technical bottlenecks of traditional electronic methods in phase noise and real-time frequency switching, various innovative solutions have been proposed in the photonics field in recent years. Significant progress has been made in technologies such as frequency–time mapping [10], space–time mapping [11], photonic frequency multiplication [12] and temporal pulse shaping [13]. However, both electronic and photonic signal generation technologies face the common challenge of phase noise degradation. Specifically, electronic synthesizers are fundamentally limited by the DAC sampling rate and clock frequency in DDS [14], or by the trade-off between loop bandwidth and phase noise in PLLs [15], making it difficult to simultaneously achieve fine frequency steps, fast switching, and low phase noise at high frequencies. Photonic waveform generation techniques such as frequency–time mapping and temporal pulse shaping are primarily open-loop architectures that inevitably suffer from phase noise degradation due to the lack of a high-Q resonant cavity [16]. In contrast, utilizing optical frequency combs (OFC) or OEO to generate FA signals offers greater advantages in low-noise performance [17,18], making them promising methods for photonic generation of frequency-agile microwaves. Nevertheless, they still suffer from the common problem of limited flexibility in frequency agility.

The optoelectronic oscillator (OEO) is a self-excited oscillation system based on optical energy storage devices, which adopts a closed-loop optoelectronic hybrid structure with a high-Q fiber ring cavity as its core [19]. The long delay characteristic of the fiber ring cavity provides strong suppression of phase noise, so the OEO has the ability to generate high-purity microwave signals. The Fourier domain mode-locked optoelectronic oscillator (FDML-OEO) has been developed in recent years [20–22]. Using frequency-domain phase-locking technology, it can excite a large number of longitudinal modes with fixed phase relationships in the Fourier domain and directly generate periodic linear frequency modulated (LFM) signals [23,24]. Compared with conventional time-domain oscillation schemes, this method breaks through relevant restrictions and can generate chirped signals with a large time-bandwidth product. However, the FDML-OEO still has obvious limitations. It can only produce periodic signals, and its performance is greatly affected by the loop transmission delay, which includes the total delay of all optoelectronic components. This greatly restricts the flexibility of microwave signal output, particularly for applications that demand fast frequency reconfiguration and aperiodic frequency-agile operation.

In this work, we design and experimentally validate an FA optoelectronic hybrid oscillator that can generate aperiodic microwave signals with rapid frequency tuning. Within the oscillation loop, a FA filtering unit is built based on a delay-matched mixing structure and a programmable local oscillator (LO) [25,26]. To address the frequency mismatch induced during frequency hopping, a real-time frequency compensation module is adopted to maintain stable mode transition. Meanwhile, a precisely designed link delay-matching unit is utilized to reduce the impact of LO phase noise on the output signal. As a result, the phase noise of the generated signal is optimized to around −120 dBc/Hz at 10 kHz offset, which well balances fast switching speed and high spectral purity. More importantly, the proposed structure breaks the inherent frequency limitation brought by conventional loop filters in typical OEO systems. Experimental results confirm that the system realizes excellent frequency agility while preserving low phase noise and supports

arbitrary frequency tuning with a range up to 1000 times the FSR. In addition, the oscillation frequency can be finely adjusted with a minimum step of 100 kHz. Such flexible frequency tuning capability enables the system to fit complex application environments and effectively improves the anti-jamming performance and frequency adjustment range. Compared with traditional periodic chirp signals (e.g., LFM generated by FDML-OEO), aperiodic frequency-agile waveforms offer non-deterministic frequency sequences that are unpredictable to hostile interceptors. In radar and electronic countermeasure scenarios, this unpredictability prevents jamming systems from tracking or predicting the transmitted spectrum, thereby significantly lowering the probability of intercept and improving the anti-jamming margin.

2. Methods

The schematic principle of the proposed scheme is presented in Figure 1. For a clearer illustration of its operating mechanism, we make a comparative analysis with the conventional FDML-OEO configuration. As depicted in Figure 1a, the proposed oscillator features a streamlined structural design along with the time-dependent frequency response of the output signal, where an aperiodic frequency-agile filter and an in-phase/quadrature (IQ) modulation unit are incorporated to perform instantaneous frequency compensation. Figure 1b plots the FDML-OEO model that produces periodic signals. Unlike the proposed scheme, this structure employs a conventional periodic linear filter inside the oscillation loop.

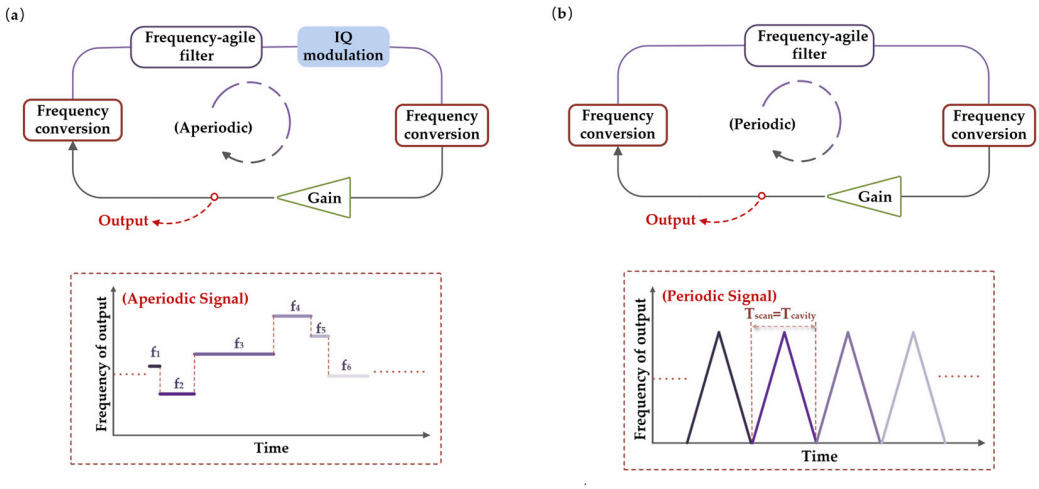

Figure 1. Structural comparison and corresponding output characteristics of the two oscillators. (**a**) Configuration of the proposed optoelectronic hybrid oscillator and time–frequency behavior of its output signal; (**b**) architecture of the conventional FDML-OEO system and periodic frequency form of the FDML-OEO output.

Specifically, the actual links of both structures can be generally summarized as a combination of three parts: a frequency conversion module, a gain module, and a filter module, but there are essential differences in their core working mechanisms and oscillation principles.

In the traditional OEO structure, a filter in the loop is used to select frequencies that satisfy the oscillation phase condition, and then a gain module is employed to make the mode oscillate back and forth in the cavity, ultimately achieving stable microwave signal generation. This basic model is established based on the PBC [19], which can be expressed as follows:

$$S_{osc-p}(t) = G\left(\left|S_{osc-p}\right|\right)S_{osc-p}(t-\tau_L) + n(t), \quad (1)$$

where $S_{osc-p}(t)$ is the oscillation periodic output, $G(|S_{osc-p}|)$ is the effect of gain on the transmitted signal, τ_L denotes the delay introduced by the signal during transmission through the loop, and $n(t)$ is the additional phase noise of the loop. When the system continuously outputs a stable oscillation signal (i.e., the gain is approximately 1), the frequency variation of the signal derived satisfies $f_{osc-p}(t) = f_{osc-p}(t - \tau_L)$. This means that the round-trip signal must be periodic and strictly bound to the loop delay, which greatly limits its flexible adjustment ability. Therefore, although the FDML-OEO can generate LFM signals, the scanning period of the signal center frequency is strictly synchronized with the cavity length requirement, and the output can only be in a fixed form within each period.

To achieve the output of arbitrarily frequency-agile signals, the proposed oscillator setup innovatively incorporates an aperiodic dynamic filter whose filtering frequency exhibits obvious aperiodic transition characteristics over time. Meanwhile, the model introduces a dedicated dynamic frequency compensation unit composed of IQ modulation to effectively suppress frequency shift and guarantee stable mode switching. The transformation process of the signal during transmission in the loop is

$$S_{osc-ap}(t) = G(|S_{osc-ap}|)S_{osc-ap}(t - \tau_L)h_{IQ}(t) + n(t). \quad (2)$$

Here, $h_{IQ}(t)$ denotes the functional influence exerted by the IQ modulation unit. Suppose the instantaneous oscillation frequency of the modified system is defined as $f_{osc-ap}(t)$. When the compensation frequency $f_{IQ}(t)$ is configured to match the real-time frequency difference of the oscillating signal, i.e.,

$$f_{IQ}(t) = [f_{osc-ap}(t) - f_{osc-ap}(t - \tau_L)], \quad (3)$$

Under this configuration, the oscillation frequency is no longer tied to the loop delay τ_L. The combined operation of the aperiodic dynamic filter and the IQ-enabled frequency compensation unit allows different oscillation modes to retain high-frequency stability throughout round-trip transmission within the cavity. Consequently, the periodic constraint imposed by the loop delay is completely eliminated, enabling flexible frequency agility with arbitrary temporal sequences.

3. Results

3.1. Experimental Setup

The overall experimental setup of the proposed scheme is schematically shown in Figure 2a. The entire experimental platform is built around a closed-loop oscillation framework, which integrates a reconfigurable FA filter and a real-time frequency compensation module. The core filtering part is marked with a yellow dashed box in the diagram. Adopting a delay-matched mixing pair architecture, the whole system is functionally partitioned into three parallel transmission branches: LO, intermediate frequency (IF), and radio frequency (RF) paths.

As the core of the oscillation loop, an optoelectronic hybrid aperiodic dynamic filter with delay-matching capability is deployed within the LO and IF branches. The dual-channel AWG (Keysight M8190A) is configured to operate at a sampling rate of 10 GSa/s, with both channels sharing a common internal clock and trigger source to ensure deterministic phase synchronization. Channel 1 (CH1) generates the aperiodic frequency-agile LO waveform; its output frequency is arbitrarily configured such that, after up-conversion with the IF signal, the resulting oscillation falls within the passband of the RF filter (centered at 2 GHz with a bandwidth of 220 MHz). The output power of CH1 is set to −17 dBm and is subsequently amplified by a 30 dB low-noise amplifier (LNA) before being split into two independent branches for subsequent processing. Channel 2 (CH2) generates the real-time

phase-compensation waveform that drives the IQ modulator. Based on the pre-measured loop delay, CH2 is calculated to produce a signal whose phase equals the differential frequency between the instantaneous CH1 and its delayed replica according to Equation (3), thereby compensating for the phase distortion arising during frequency hopping.

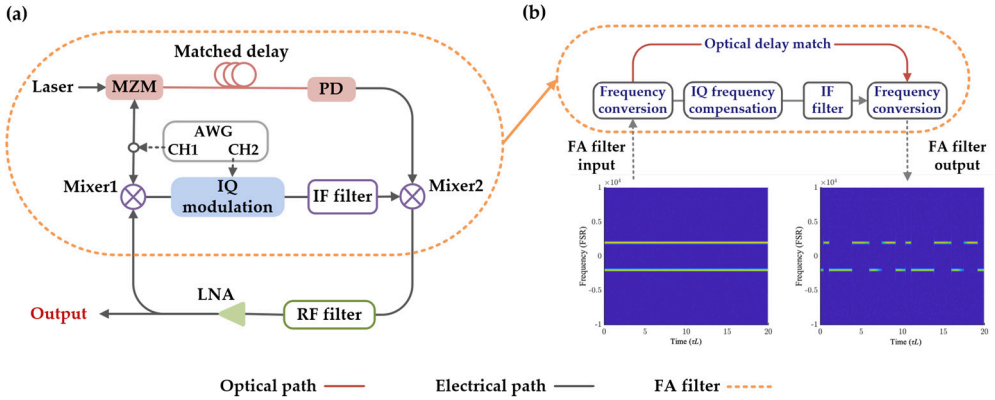

Figure 2. (**a**) Experimental setup with the FA filter in the dashed box; (**b**) VNA measurement of the input and output of the FA filter, with a total measurement duration of twice the period of the signal.

One branch of the amplified LO signal is sent to the optical delay link for delay matching, aiming to weaken the degradation effect of LO phase noise on the generated RF signal. A laser with an output power of 13 dBm provides a stable optical carrier, which is modulated by the LO signal via a Mach–Zehnder modulator (MZM, 20 GHz bandwidth, EOSPACE, Redmond, WA, USA). After propagating through the optical fiber delay line, the modulated optical signal is converted back to the electrical domain by a photodetector (Analog PIN Photodetector, DSC40S, 14 GHz bandwidth, Discovery Semiconductors, Ewing, NJ, USA), which offers a 3-dB bandwidth of 14 GHz. The key design principle of the optoelectronic delay-matching module is to ensure that the time delay introduced by the 2 km optical fiber is approximately equal to the group delay generated by the IF filter centered at 124.8 MHz. The recovered electrical signal is then up-converted with the filtered IF signal. The mixed signal is further filtered by a band-pass RF filter to remove unwanted spurious signals and intermodulation components, which introduces an insertion loss of about 5 dB. The small-signal loop gain is primarily provided by a low-noise amplifier with 33 dB gain, ensuring stable self-sustained oscillation.

The other branch of the LO signal from CH1 is down-converted with the loop oscillation signal, and the obtained IF signal inevitably exhibits frequency distortion caused by the inherent transmission delay in the RF path.

To eliminate such distortion and ensure stable signal hopping, the driving signal generated by CH2 of the AWG is applied to the IQ modulator to implement real-time frequency compensation and maintain continuity during aperiodic frequency switching. According to Equation (3), the CH2 compensation signal is determined by the loop delay τ_L, which is pre-measured by a vector network analyzer (VNA). The dual-channel AWG shares a common clock, ensuring that the CH2 phase-compensation waveform arrives at the IQ modulator synchronously with the down-converted signal, thereby canceling the phase discontinuity. The above energy transmission and signal processing procedures constitute a complete closed-loop oscillation mechanism and finally enable the stable generation of high-performance FA microwave signals.

The signal transmission process from the input of Mixer 1 to the output of Mixer 2 constitutes the core FA filter of the system, which is critical to achieving a dynamic aperiodic signal output. We characterized the transmission response of the proposed filter using a VNA and illustrated the time–frequency evolution of the signal from the filter input to the

output. The measurement results are presented in Figure 2b. The time axis is determined by the loop delay of the system. The measured loop delay τ_L is approximately 10 microseconds, corresponding to an FSR of around 100 kHz. The dual-frequency signal injected into Mixer 1 possesses a wide frequency span up to 1000 times the FSR. After passing through the FA filter, the signal exhibits clear aperiodic dynamic frequency variation characteristics. The measurement results show that by properly configuring the waveform of CH1, the signal output from the oscillation loop can generate signals with random frequency components and arbitrary durations. Moreover, the frequency switching response is independent of the bandwidth and response speed of the IF filter.

3.2. Experimental Results

Random-frequency LO signals are injected via CH1 in experiments to examine the frequency-agile performance of the developed oscillator structure. Figure 3 displays comparative time–frequency results under different working conditions, where the frequency coordinate takes loop FSR as the measurement unit and sets the 2 GHz central frequency of the RF filter as the zero reference. The whole observation period spans 100 cavity round-trip delays.

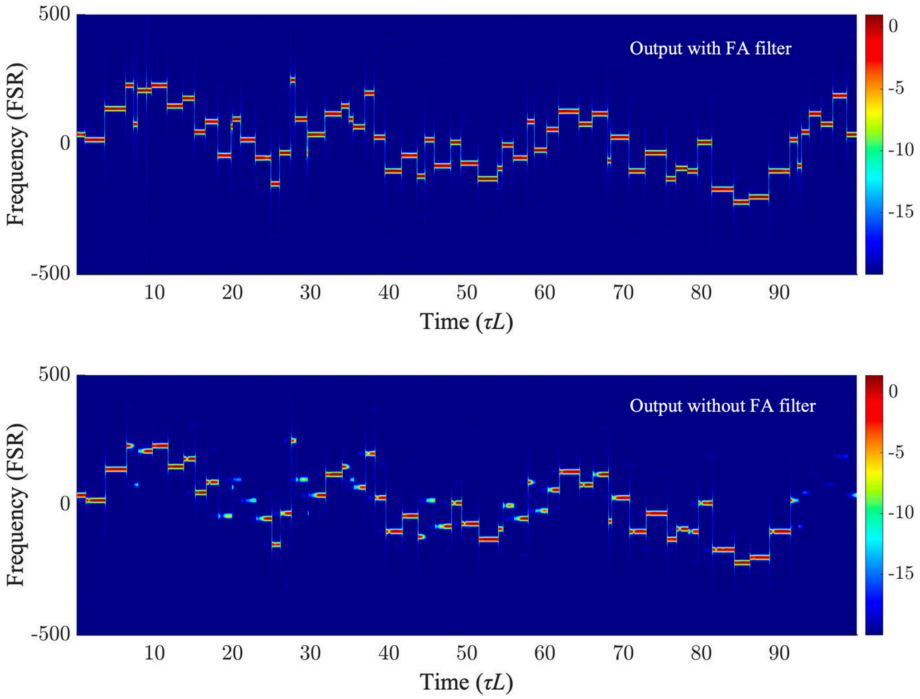

Figure 3. Time–frequency characteristics of output signals with and without frequency-agile filter. The observation time spans 100 loop round-trip delays, and the 2 GHz serves as the zero reference frequency.

Distinct output behaviors can be observed between the two test cases. Equipped with the designed FA filter, the system achieves a desirable aperiodic frequency-agile output. Each frequency component lasts randomly from 1 μs to 28 μs, breaking the inherent periodic limitation of conventional oscillators that can only generate signals related to non-integer multiples of loop delay. By contrast, the signal obtained without FA filtering shows evident frequency discontinuity. The oscillation mode cannot be reconstructed rapidly during frequency switching, presenting an unstable operating status. The obvious performance gap fully proves that the introduced filtering structure enables stable and flexible aperiodic output and greatly improves signal switching quality.

To comprehensively evaluate spectral profiles, amplitude stability and time–frequency evolution of the output microwave signal, relevant signal acquisition and analysis are implemented. A dual-frequency hopping LO signal lasting 2.28 loop delays is adopted to study the system oscillation behaviors. The system ultimately yields stable microwave signals centered at 2 GHz with an effective bandwidth of 100 MHz. All analytical results are illustrated in Figure 4.

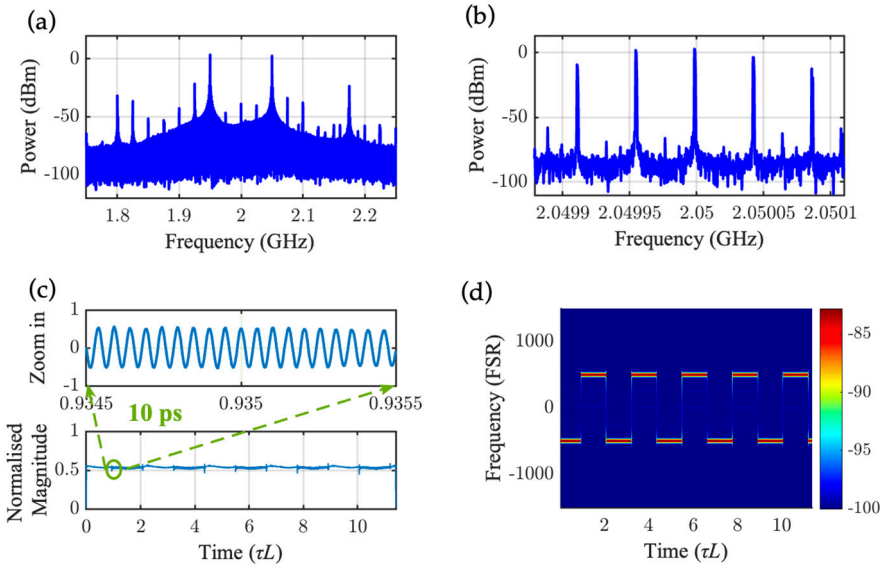

Figure 4. Experimental observation results of a dual-frequency agile signal with a period of 2.28 times the loop length. (**a**) Power spectral density distribution of the signal; (**b**) partial zoom-in of the spectral characteristics in (**a**), focusing on presenting the spectral line details; (**c**) time-domain amplitude characteristics of the signal and the zoom-in results of the waveform in the key transition region; (**d**) time–frequency analysis results.

The overall spectrum measured by Keysight N9030B spectrum analyzer is plotted in Figure 4a, with signal energy predominantly gathered at two hopping frequency points. The zoomed spectral view in Figure 4b shows a line interval of 43.8 kHz, which coincides with the 22.8 μs tuning cycle of the driving signal. Waveform data is acquired by a 20 GSa/s oscilloscope, as illustrated in Figure 4c,d. Figure 4c characterizes the amplitude profile of signals, and the inset magnified view verifies steady amplitude output free of waveform interruption. Figure 4d shows dynamic time–frequency evolution, where frequency trajectories maintain high continuity during switching procedures. The above experimental evidence demonstrates that the developed system can produce high-quality aperiodic frequency-agile signals, and the measured performance matches well with the theoretical design.

3.3. Phase Continuity and Stability

For a clearer characterization of the phase retention stability of signals generated by the system, statistical and quantitative phase measurements are carried out on the signal spanning a total duration of 500 cavity oscillation periods. Using the system's fundamental oscillation frequency as the reference, the average phase of the frequency-agile signal relative to the reference is extracted period by period. Time-domain fluctuation curves of the average phase are plotted for the two hopping frequencies in their respective operating cycles, and the root mean square error (RMSE) of phase fluctuation is calculated to quantify the phase stability. The results are shown in Figure 5, in which the two colored curves represent the average phase variation at different operating frequencies. The legend

indicates the error range of phase mean fluctuation and the corresponding RMSE calculation results for the two cases.

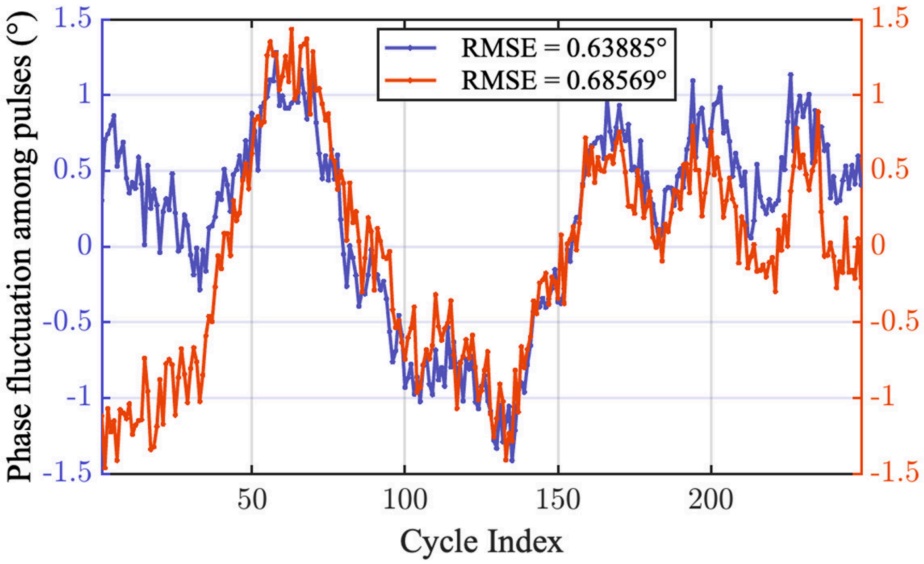

Figure 5. Period-averaged phase fluctuations of two frequencies during hopping. The temporal variations of the average phase of the two target frequencies over 250 consecutive cavity oscillation cycles during aperiodic random frequency hopping. The legend marks the RMSE of phase fluctuations for each frequency.

Experimental results show that during aperiodic random frequency agile, the carrier phase remains highly consistent whenever switching back to the same frequency point, with no obvious phase jump or random discrete phenomenon. After the DC component of phase fluctuation is eliminated, the obtained RMSE value is extremely small, which fully confirms that the frequency hopping achieves phase-level continuous stability. Different from conventional oscillators with random phase reset after each frequency switching, the oscillation loop maintains uninterrupted continuous operation instead of intermittent restart oscillation, which fundamentally ensures the phase coherence of frequency-agile signals.

We analyze the influence mechanism of LO noise on output and investigate the phase noise characteristics of final waveforms. Relevant theoretical conclusions are verified by experimental measurements. The adopted loop filter incorporates a delay-matched mixing pair. This design not only enables dynamic frequency selection but also suppresses LO phase noise interference by precisely tuning the delay difference between LO and IF paths.

Neglecting other frequency conversion processes, the pure LO signal is denoted as $S^N_{CH1}(t)$, with its phase noise defined as $\varphi_{NCH1}(t)$. Here, the superscript N indicates the noise-corrupted signal, including the LO phase-noise contribution. With the excitation of local oscillator signals, the input–output relationship of signals passing through the FA filter is given by the formula below:

$$S^N_{out}(t) = G\left(\left|S^N_{in}\right|\right)\left[S^N_{in}(t)S^*_{CH1}(t-\tau_{IF})e^{i\varphi_{NCH1}(t-\tau_{IF})}\right]S_{CH1}(t-\tau_O)e^{-i\varphi_{NCH1}(t-\tau_O)}. \quad (4)$$

In the above formula, when the delay τ_{IF} introduced by the IF link equals the compensation delay τ_O of the optical fiber link, the phase noise terms of the LO cancel each other out during two frequency conversions. Consequently, no extra phase noise carried by the local oscillator will be superimposed on the final microwave signal.

Meanwhile, we derive the final phase noise formula of signals generated in the loop. When oscillating signals propagate back and forth within the closed loop, $S^N_{OSC}(t)$ represents the ideal oscillation signal without phase noise, and $\varphi_N(t)$ stands for the phase

noise component. Under well-matched delay conditions of the FA filter, substituting the compensation phase term of the dynamic phase shifter into Equation (3), the microwave signal at the output satisfies the following formula:

$$S_{OSC}^{N}(t)e^{-i\varphi_N(t)} = G\left(\left|S_{OSC}^{N}\right|\right)\left[S_{OSC}^{N}(t-\tau_L)e^{-i\varphi_N(t-\tau_L)}\right] + n_A(t). \quad (5)$$

In addition to the LO phase noise, the optical link inevitably introduces additive noise during electro-optical and optical-electrical conversions, including the laser relative intensity noise (RIN), photodetector shot noise, and thermal noise from RF amplifiers. However, as expressed by Equation (5), once the LO phase noise is eliminated by the delay-matched mixing pair, the residual noise term $n_A(t)$ propagates through the feedback loop in the same form as the classical Yao–Maleki OEO model. Consequently, the phase-noise performance of the proposed architecture is governed by the high-Q cavity storage rather than by the optical-link noise floor. Under the present experimental conditions, the combined broadband noise floor contributed by the optical link is well below the measured output phase noise, indicating that the system preserves the intrinsic low-phase-noise advantage of conventional OEOs. This proves that the phase noise performance of the experimentally generated signals matches that of fixed-frequency oscillating signals.

The above theoretical analysis is verified by experimental results, as illustrated in Figure 6. Figure 6a,b show the spectra obtained using a continuous-wave signal and a frequency-hopping signal as the LO, respectively. Owing to the characteristics of the mixing pair structure, the phase noise of the oscillating signals relative to the LO is attenuated by 13 dB in both oscillator operating modes. In the single-frequency mode, the phase noise of the generated signal at a 10 kHz offset from the carrier is approximately −121 dBc/Hz, whereas the measured phase noise at the same frequency offset in the frequency-agile mode is about −118 dBc/Hz, with a deviation of roughly 3 dB.

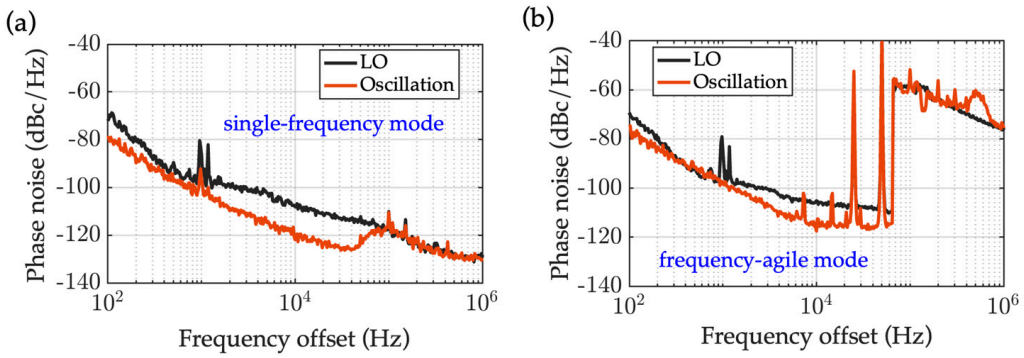

Figure 6. Phase noise measurement results in single-frequency mode and frequency-agile mode. (**a**) Phase noise results of the oscillation signal and LO signal under single-mode oscillation; (**b**) phase noise results of the oscillation signal and LO signal under frequency-agile oscillation.

Analysis indicates that this difference is mainly attributed to the degradation of the signal-to-noise ratio (SNR) caused by the reduction in signal power. When characterizing the phase noise of frequency-agile signals using a spectrum analyzer, only the signal power at a single operating frequency can be acquired in each measurement. The measured results demonstrate that the output power in the frequency-agile mode is reduced by half compared with that in the single-frequency oscillation mode owing to frequency hopping. Based on the theoretical phase noise formula, the decrease in carrier power directly gives rise to phase noise degradation under the same noise power, which quantitatively accounts for the measurement discrepancy between the two operation modes. The phase noise measurement results of the LO input present a similar deviation, and the underlying

mechanism is consistent with the above analysis. A comparison between Figure 6a,b illustrates that the frequency-agile and single-frequency signals exhibit intrinsic consistency in their phase noise characteristics, which fully validates that the proposed system can maintain superior phase noise performance during the entire mode-switching process.

4. Conclusions

This study presents a novel FA optoelectronic hybrid oscillator architecture that breaks the technical limitations of conventional schemes such as FDML-OEO, which depend on the PBC. The proposed architecture innovatively incorporates an aperiodic dynamic filter and a real-time frequency compensation mechanism, successfully generating frequency-agile microwave signals capable of random hopping to arbitrary preset frequencies within a non-integer multiple of the cavity round-trip time. The feasibility of the scheme is verified through theoretical analysis, and experimental results confirm that the generated signals can oscillate stably inside the cavity. The structural advantages of the architecture ensure excellent phase noise performance of the output signal. The aperiodic frequency arrangement demonstrated in this work provides unique advantages in electronic countermeasure applications, where non-repetitive hopping patterns are essential for evading intelligent jamming and spectrum surveillance. This work provides a new technical paradigm for application scenarios requiring rapid frequency reconstruction, such as radar systems and cognitive radio, and its aperiodic frequency arrangement characteristic has unique advantages in the field of anti-jamming communication.

Author Contributions: Conceptualization, T.Y. and Y.D.; methodology, T.Y.; software, T.Y.; validation, T.Y., Y.L. and T.H.; formal analysis, T.Y. and Y.L.; investigation, T.H.; resources, F.Y. and M.L.; data curation, T.Y.; writing—original draft preparation, T.Y.; writing—review and editing, T.Y., T.H. and Y.D.; visualization, T.Y.; supervision, T.Y.; project administration, Y.D. and K.X. All authors have read and agreed to the published version of the manuscript.

Funding: This work was supported by the National Natural Science Foundation of China (62135014).

Institutional Review Board Statement: Not applicable.

Informed Consent Statement: Not applicable.

Data Availability Statement: Data is contained within the article.

Conflicts of Interest: The authors declare no conflicts of interest.

Abbreviations

The following abbreviations are used in this manuscript:

OEO	Optoelectronic Oscillator.
FDML-OEO	Fourier Domain Mode-Locked Optoelectronic Oscillator.
PBC	Periodic Boundary Condition.
RF	Radio Frequency.
LNA	Low-Noise Amplifier.
FSR	Free Spectral Range.
IF	Intermediate Frequency.
FA	Frequency-Agile.
LO	Local Oscillator.
SNR	Signal-to-Noise Ratio.
PD	Photodetector.
AWG	Arbitrary Waveform Generator.
IQ	In-phase/Quadrature.

References

1. Pan, S.; Zhang, Y. Microwave Photonic Radars. *J. Light. Technol.* **2020**, *38*, 5450–5484. [CrossRef]
2. Salama, A.A.; Hussein, M.A. Enhanced projectile path estimation using multi-vehicle FMCW radar sensors: AA Salama, MA Hussein. *Sci. Rep.* **2026**, *16*, 4533. [CrossRef] [PubMed]
3. Reddy, R.; Sinha, S. State-of-the-art review: Electronic warfare against radar systems. *IEEE Access* **2025**, *13*, 57530–57567. [CrossRef]
4. Pan, Y.; Xie, D.; Zhao, Y.; Wang, X.; Huang, Z. Overview of radar jamming waveform design. *Remote Sens.* **2025**, *17*, 1218. [CrossRef]
5. Yu, Z.; Hao, Z.; Yao, W.; Jia, M. A Capacity Enhancement Method for Frequency-Hopping Anti-Jamming Communication Systems. *Electronics* **2023**, *12*, 4457. [CrossRef]
6. Wu, Q.H.; Wang, H.Q.; Li, X.; Zhang, B.; Peng, J.L. Reinforcement Learning-Based Anti-Jamming in Networked UAV Radar Systems. *Appl. Sci.* **2019**, *9*, 5173. [CrossRef]
7. Hanbali, S.B.S. A review of radar signals in terms of Doppler tolerance, time-sidelobe level, and immunity against jamming. *Int. J. Microw. Wirel. Technol.* **2018**, *10*, 1134–1142. [CrossRef]
8. Zhou, P.; Jiang, Z.; Tang, Z.; Li, N.; Pan, S. Microwave Phase Noise Analyzer Based on Photonic Delay-Matched Frequency Translation. *IEEE Trans. Microw. Theory Tech.* **2024**, *72*, 5498–5506. [CrossRef]
9. Uusikartano, R.; Niittylahti, J. A digital frequency synthesizer for a 2.4 GHz fast frequency hopping transceiver. In *Proceedings of the 43rd IEEE Midwest Symposium on Circuits and Systems (Cat. No. CH37144), Lansing, MI, USA, 8–11 August 2000*; IEEE: New York, NY, USA, 2000; pp. 420–423.
10. Liu, Q.; Fok, M.P. Ultrafast and wideband microwave photonic frequency-hopping systems: A review. *Appl. Sci.* **2020**, *10*, 521. [CrossRef]
11. McKinney, J.D.; Seo, D.; Leaird, D.E.; Weiner, A.M. Photonically assisted generation of arbitrary millimeter-wave and microwave electromagnetic waveforms via direct space-to-time optical pulse shaping. *J. Light. Technol.* **2003**, *21*, 3020. [CrossRef]
12. Li, S.; Cui, Z.; Ye, X.; Feng, J.; Yang, Y.; He, Z.; Cong, R.; Zhu, D.; Zhang, F.; Pan, S. Chip-based microwave-photonic radar for high-resolution imaging. *Laser Photonics Rev.* **2020**, *14*, 1900239. [CrossRef]
13. Yang, Z.; Liu, Z.; Jiang, Y.; Liu, H.; Li, J.; Dong, W. High-precision photonics-assisted two-step microwave frequency measurement combining time and power mapping method. *Sensors* **2024**, *24*, 6415. [CrossRef] [PubMed]
14. Tierney, J.; Rader, C.; Gold, B. A digital frequency synthesizer. *IEEE Trans. Audio Electroacoust.* **2003**, *19*, 48–57.
15. Gardner, F.M. *Phaselock Techniques*; John Wiley & Sons: Hoboken, NJ, USA, 2005.
16. Chen, J.-Q.; Chen, C.; Sun, J.-J.; Zhang, J.-W.; Liu, Z.-H.; Qin, L.; Ning, Y.-Q.; Wang, L.-J. Linewidth measurement of a narrow-linewidth laser: Principles, methods, and systems. *Sensors* **2024**, *24*, 3656. [CrossRef] [PubMed]
17. Blatnik, A.; Zmrzlak, L.; Batagelj, B. Radio Front-End for Frequency Agile Microwave Photonic Radars. *Electronics* **2024**, *13*, 4662. [CrossRef]
18. Liu, Y.; Zhang, Z.; Burla, M.; Eggleton, B.J. 11-ghz-bandwidth photonic radar using mhz electronics. *Laser Photonics Rev.* **2022**, *16*, 2100549. [CrossRef]
19. Yao, X.S.; Maleki, L. Optoelectronic microwave oscillator. *J. Opt. Soc. Am. B* **1996**, *13*, 1725–1735. [CrossRef]
20. Zhou, P.; Zhang, F.; Pan, S. Generation of linear frequency-modulated waveforms by a frequency-sweeping optoelectronic oscillator. *J. Light. Technol.* **2018**, *36*, 3927–3934. [CrossRef]
21. Yi, Z.; Wo, J.; Zhang, J.; Yao, J. Time Duration Tunable Fourier Domain Mode-Locked Optoelectronic Oscillator Based on a Frequency Shifting Loop. In Proceedings of the 2023 Opto-Electronics and Communications Conference (OECC), Shanghai, China, 2–6 July 2023; pp. 1–3.
22. Hao, T.; Cen, Q.; Dai, Y.; Tang, J.; Li, W.; Yao, J.; Zhu, N.; Li, M. Breaking the limitation of mode building time in an optoelectronic oscillator. *Nat. Commun.* **2018**, *9*, 1839. [CrossRef] [PubMed]
23. Ma, R.; Huang, Z.; Yao, X.S.; Hao, P.; Ke, W.; Cai, X. V-band ultra-fast tunable thin-film lithium niobate Fourier-domain mode-locked optoelectronic oscillator. *Light Sci. Appl.* **2025**, *14*, 398. [CrossRef] [PubMed]
24. Zhang, L.; Wu, Y.; Tian, H.; Zeng, Z.; Zhang, Y.; Zhang, Z.; Zhang, Y.; Zhang, S.; Li, H.; Liu, Y. Mode locking mechanism in Fourier-domain mode-locked optoelectronic oscillators. *Opt. Express* **2024**, *32*, 40074–40091. [CrossRef] [PubMed]
25. Guan, S.; Cen, Q.; Yin, F.; Xu, K.; Dai, Y. Low spurious optoelectronic oscillator achieved by frequency conversion filtering without deteriorating phase noise. *Opt. Express* **2020**, *28*, 18529–18537. [CrossRef] [PubMed]
26. Dai, Y.; Wang, R.; Yin, F.; Dai, J.; Zhou, Y.; Li, J.; Xu, K. Hybrid radio-intermediate-frequency oscillator with photonic-delay-matched frequency conversion pair. *Opt. Lett.* **2015**, *40*, 2894–2897. [CrossRef] [PubMed]